ELSEVIER

Journal of Structural Geology 29 (2007) 1256–1266

JOURNAL OF STRUCTURAL GEOLOGY

www.elsevier.com/locate/jsg

# Using differential geometry to describe 3-D folds

Ian Mynatt [a], Stephan Bergbauer [b], David D. Pollard [a,*]

[a] *Department of Geological and Environmental Sciences, Stanford University, 450 Serra Mall, Bldg 320, Stanford, CA 94305, USA*
[b] *BP Exploration (Alaska) Inc., P.O. Box 196612 Anchorage, Alaska 99519-6612, USA*

Received 13 March 2006; received in revised form 19 January 2007; accepted 2 February 2007
Available online 20 February 2007

**Abstract**

We provide methods to objectively characterize 3-D folds and present applications for different fold types at varying scales and formed in different tectonic settings. Algorithms based on differential geometry quantify all geometric aspects of the surfaces. The geologic curvature classification defines the shape and orientation of points on the folded surface. The curvature threshold introduces a method to extract geologically significant aspects of fold shape by disregarding curvature magnitudes less than a certain value. This permits the evaluation of the cylindricity of the folded surface at particular points.


*Keywords:* Fold; Fold classification; Three dimensional folds; Differential geometry; Curvature; Gaussian curvature; Mean curvature; Geologic curvature

## 1. Introduction

Folds and the mechanics of folding have attracted the attention of structural geologists for over a century (e.g., Gilpin, 1883; Cloos, 1936; Ramberg, 1961; Ramsay, 1967; Stearns, 1969; Johnson, 1977; Davis, 1979; Treagus and Treagus, 1981; Suppe, 1983; Dunne, 1986; Ramsay and Huber, 1987; Suppe and Medwedeff, 1990; Johnson and Fletcher, 1994; Bobillo-Ares et al., 2000; Maxelon and Mancktelow, 2005). A necessary first step of such an investigation is a description of the fold geometry, whether as a constraint for kinematic tectonic reconstruction or to prescribe boundary conditions on models examining the mechanics of folding. Particularly given the increase in the availability and use of 3-D data sets, such as light detection and ranging (LiDAR), global positioning systems (GPS), 3-D seismic reflection and 3-D scanning, new tools are needed to rigorously quantify both measured and modeled geometries.

We suggest that the application of differential geometry to geologic surfaces provides these new tools. Differential geometry is a mathematical framework for the quantitative description of curves and surfaces (e.g., Struik, 1961; Lipschultz, 1969; Stoker, 1969). By using differential geometry to calculate surface normal and tangent vectors, and the spatial rates of change of these quantities, mathematically rigorous geometric descriptions of geologic structures can be obtained, including various measurements of surface curvature. These complete descriptions supplant 2-D approximations based on assumptions of fold cylindricity and classical analysis techniques based on strike and dip measurements across a fold as plotted on a stereographic projection.

Curvature computations have been employed by structural geologists to describe the geometry of folded surfaces (e.g., Bengtson, 1981; Lisle, 1992; Lisle and Robinson, 1995; Roberts, 2001; Bergbauer and Pollard, 2003; Bergbauer et al., 2003; Lisle and Fernández Martínez, 2005; Pearce et al., 2006), to quantify the degree of deformation or strain in deformed strata (e.g., Bevis, 1986; Ekman, 1988; Lisle, 1994; Nothard et al., 1996; Samson and Mallet, 1997; Wynn and Stewart, 2005), and to predict fracture orientations and densities in bent strata (e.g., Murray, 1968; Thomas et al., 1974; Lisle, 1994; Fischer and Wilkerson, 2000; Hennings et al.,

* Corresponding author. Tel.: +1 650 723 4679.
*E-mail addresses:* imynatt@pangea.stanford.edu (I. Mynatt), dpollard@pangea.stanford.edu (D.D. Pollard).

0191-8141/$ - see front matter © 2007 Published by Elsevier Ltd.
doi:10.1016/j.jsg.2007.02.006

2000; Bergbauer 2002). We expand upon this research and introduce a new computational tool to aid in the structural analysis of folds.

## 2. Differential geometry and curvature

### 2.1. The first and second fundamental forms

Two partial differential equations define the so-called first and second fundamental forms of differential geometry and uniquely determine how to measure lengths, areas and angles on a surface and how to describe the shape of a parameterized surface in 3-D Euclidean space (Lipschultz, 1969, p. 171). Several explanations and derivations of these quantities focusing on applications to geologic surfaces exist, including Bergbauer and Pollard (2003), Pollard and Fletcher (2005), Pearce et al. (2006) and references therein, so only a brief treatment is given here.

Natural surfaces may be idealized either by continuous functions, or by samples at points on irregular (geologic) or regular (seismic or scanned) grids. If $z(u,v)$ is a single-valued continuous function or a set of discrete elevation measurements with respect to the $(u,v)$-parameter plane, the surface or patch of the surface can be defined as:

$$\vec{\mathbf{x}}(u,v) = u\hat{\mathbf{e}}_x + v\hat{\mathbf{e}}_y + z(u,v)\hat{\mathbf{e}}_z \tag{1}$$

Here $\vec{\mathbf{x}}$ is the position vector of every point on the surface, $u$ and $v$ are two independent parameters in the horizontal parameter plane and $(\hat{\mathbf{e}}_x, \hat{\mathbf{e}}_y, \hat{\mathbf{e}}_z)$ are the respective unit vectors in the directions of the Cartesian coordinate system axes $(x,y,z)$. Eq. (1) is the parametric form of the geologic surfaces considered here.

We consider $\vec{\mathbf{x}}$ to be a continuous function of $u$ and $v$ with well defined partial derivatives:

$$\vec{\mathbf{x}}_u = \frac{\partial \vec{\mathbf{x}}}{\partial u}, \quad \vec{\mathbf{x}}_v = \frac{\partial \vec{\mathbf{x}}}{\partial v}. \tag{2}$$

Because $\vec{\mathbf{x}} = \vec{\mathbf{x}}(u,v)$, the differential $\mathrm{d}\vec{\mathbf{x}}$ is defined:

$$\mathrm{d}\vec{\mathbf{x}} = \vec{\mathbf{x}}_u \mathrm{d}u + \vec{\mathbf{x}}_v \mathrm{d}v \tag{3}$$

Geometrically, $\mathrm{d}\vec{\mathbf{x}}$ is a differential vector quantity that is tangent to the surface in the direction defined by $\mathrm{d}u$ and $\mathrm{d}v$, and $\mathrm{d}\vec{\mathbf{x}}$ is the key to the first fundamental form (I). I is the inner product of $\mathrm{d}\vec{\mathbf{x}}$ with itself (Lipschultz, 1969):

$$\begin{aligned} \mathrm{I} &= \mathrm{d}\vec{\mathbf{x}} \cdot \mathrm{d}\vec{\mathbf{x}} = (\vec{\mathbf{x}}_u \mathrm{d}u + \vec{\mathbf{x}}_v \mathrm{d}v) \cdot (\vec{\mathbf{x}}_u \mathrm{d}u + \vec{\mathbf{x}}_v \mathrm{d}v) \\ &= (\vec{\mathbf{x}}_u \cdot \vec{\mathbf{x}}_u)\mathrm{d}u^2 + 2(\vec{\mathbf{x}}_u \cdot \vec{\mathbf{x}}_v)\mathrm{d}u\mathrm{d}v + (\vec{\mathbf{x}}_v \cdot \vec{\mathbf{x}}_v)\mathrm{d}v^2 \\ &= E\mathrm{d}u^2 + 2F\mathrm{d}u\mathrm{d}v + G\mathrm{d}v^2 \end{aligned} \tag{4}$$

Here $E$, $F$ and $G$ are the first fundamental coefficients. The coefficients have some remarkable properties, and can be used for the calculation of angles, distances, and areas on the surface (Eq. (1)) (Pollard and Fletcher, 2005).

The key to the second fundamental form, II, is the unit normal vector $\hat{\mathbf{N}}$ to a surface:

$$\hat{\mathbf{N}} = \frac{\vec{\mathbf{x}}_u \times \vec{\mathbf{x}}_v}{|\vec{\mathbf{x}}_u \times \vec{\mathbf{x}}_v|}, \quad |\hat{\mathbf{N}}| = 1 \tag{5}$$

The change in orientation of $\hat{\mathbf{N}}$ in a particular direction is related to the shape of the surface and is measured by the differential of:

$$\mathrm{d}\hat{\mathbf{N}} = \hat{\mathbf{N}}_u \mathrm{d}u + \hat{\mathbf{N}}_v \mathrm{d}v \tag{6}$$

The second fundamental form quantifies the spatial rate of change of $\hat{\mathbf{N}}$ in any direction as defined by $\mathrm{d}\vec{\mathbf{x}}$ at a point on the surface by taking the inner product of these two differential vectors.

$$\begin{aligned} \mathrm{II} &= -\mathrm{d}\vec{\mathbf{x}} \cdot \mathrm{d}\hat{\mathbf{N}} = -(\vec{\mathbf{x}}_u \mathrm{d}u + \vec{\mathbf{x}}_v \mathrm{d}v) \cdot (\hat{\mathbf{N}}_u \mathrm{d}u + \hat{\mathbf{N}}_v \mathrm{d}v) \\ &= -(\vec{\mathbf{x}}_u \cdot \hat{\mathbf{N}}_u)\mathrm{d}u^2 - 2(\vec{\mathbf{x}}_u \cdot \hat{\mathbf{N}}_v + \vec{\mathbf{x}}_v \cdot \hat{\mathbf{N}}_u)\mathrm{d}u\mathrm{d}v - (\vec{\mathbf{x}}_v \cdot \hat{\mathbf{N}}_v)\mathrm{d}v^2 \\ &= L\mathrm{d}u^2 + 2M\mathrm{d}u\mathrm{d}v + N\mathrm{d}v^2 \end{aligned} \tag{7}$$

Here the negative sign is by convention and $L$, $M$ and $N$ are the second fundamental coefficients which can be used to characterize the local shape of the folded surface as elliptic (dome or basin), parabolic (cylindrical fold) or hyperbolic (saddle) (Pollard and Fletcher, 2005). The ratio of fundamental forms II/I defines the normal curvature in all directions at any point on the surface.

### 2.2. Normal curvature of a surface

The concept of curvature, while intuitive for a plane curve (the reciprocal of the radius of curvature), requires a more comprehensive definition for a surface. Through a point on a surface any number of curves may be drawn with each having a different curvature at the point. The curvatures discussed here are normal curvatures, $\vec{\mathbf{k}}$, or those corresponding to curves on the surface whose curvature vectors are parallel to the normal vectors of the surface (Bergbauer and Pollard, 2003). The magnitude of the normal curvature is the scalar curvature $k$. The example of the half-cylinder (Fig. 1) shows that at a particular point on the surface, the scalar curvature can have different values depending on direction. For example, in the direction of the half-cylinder's axis (parallel to $x$), the surface has zero scalar curvature, $k = 0$. This is the smallest curvature value at any point on the surface, and therefore $k = k_{\min}$ in this direction. For a curve on the half-cylinder's surface parallel to the $(y,z)$ plane, the cylinder has uniform scalar curvature. In fact this curvature is the greatest possible on the surface, so that $k = k_{\max}$ in this direction. These extreme values are called the principal curvatures. For a curve on the surface not in one of these directions, the scalar curvature is greater than $k_{\min}$ and less than $k_{\max}$ (Fig. 1).

Following the method of Pearce et al. (2006), the orientations and magnitudes of the principle curvatures may be calculated using the first and second fundamental coefficients

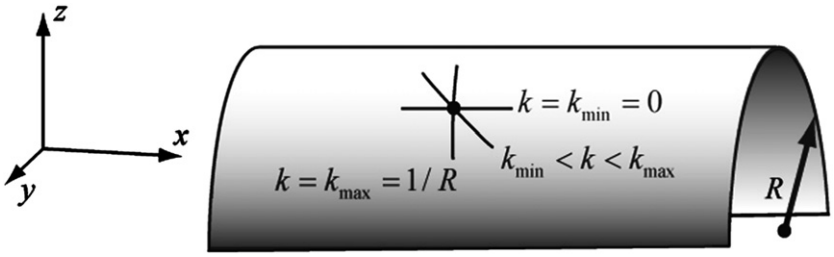


Fig. 1. Half-cylinder of radius $R$. The scalar curvature values at a point on the surface are shown for various directions.

(Henderson, 1998). At each grid point where these values are known two matrices are created, the matrix of the first fundamental form:

$$\mathbf{I} = \begin{pmatrix} E & F \\ F & G \end{pmatrix} \tag{8}$$

and the matrix of the second fundamental form:

$$\mathbf{II} = \begin{pmatrix} L & M \\ M & N \end{pmatrix} \tag{9}$$

From these the so-called shape operator may be calculated:

$$\mathbf{L} = \mathbf{I}^{-1}\mathbf{II} \tag{10}$$

where $\mathbf{I^{-1}}$ is the inverse of the matrix $\mathbf{I}$.

The magnitudes of the principle curvatures at the given point are the eigenvalues of $\mathbf{L}$ while the orientations of the principle curvatures in the parameter plane are the associated eigenvectors of $\mathbf{L}$. The author's MATLAB codes for the calculations in this paper are available at: http://pangea.stanford.edu/projects/structural_geology/chapters/chapter03/index.html.

In the case of the half-cylinder $k_{max}$ is the reciprocal of the radius $R$ of the cylinder (Fig. 1), and in general the radius of curvature and scalar curvature are related as $R = 1/k$.

The radius of curvature is an insightful measure of the curvature of a surface in a particular direction. While the radius of curvature has units of length (m), the units of curvature are inverse length ($m^{-1}$). For the rest of this paper, measurements of curvature are given first followed by the associated radius of curvature in parentheses. Because such distinctions are useful in a geologic context, convex upward surfaces have arbitrarily been assigned positive curvature values and concave upward surfaces are assigned negative values.

### 2.3. Geologic curvature and the curvature threshold

One measure of curvature already used to some extent in geologic applications (Lisle, 1994; Bergbauer, 2002; Mallet, 2002) is the Gaussian curvature $k_G = k_{min}k_{max}$. If the Gaussian curvature equals zero at a point, then at least one of the principal curvatures must be zero. If only one principal curvature is zero, the surface locally is cylindrically shaped and is either synformal or antiformal. If both principal curvatures are zero, the surface is locally planar. If $k_G < 0$, then the signs of the two principal curvatures are opposite, and the surface locally forms a saddle. If $k_G > 0$, then the two principal curvatures have the same sign and the surface at this point will have a local extremum, making it either a dome or basin.

In a geologic context, it is often important to indicate the orientation of a structure, e.g. basin versus dome. We therefore introduce the concept of geologic curvature, which expands upon the classification schemes of Roberts (2001) and Bergbauer (2002) by including variously oriented saddles as suggested by Lisle (2004, figure 3.17). The orientation of a point can be determined using the mean curvature, $k_M = (k_{min} + k_{max})/2$. By defining the Gaussian and mean curvatures at a point on a surface, the shape and orientation can be described (Lisle and Toimil, unpublished). Fig. 2 shows the geologic curvature classification scheme for points on a surface as a function of the mean and Gaussian curvature. For the half-cylinder (Fig. 1) the Gaussian and mean curvatures are $k_G = (0)(1/R) = 0$ and $k_M = (1/2)(0 + 1/R) > 0$. Using the geologic curvature classification, the half-cylinder is an antiform. This scheme is congruous with and complementary to the more mathematically oriented one presented by Lisle and Toimil (unpublished), wherein the domes and basins of Fig. 2 are classified as synclastic antiforms and synforms respectively and the antiformal and synformal saddles are classified as anticlastic antiforms and synforms respectively.

The geologic curvature classification differs from that of Lisle and Toimil (unpublished) by including idealized forms, such as the cylindrical antiform and synform, the plane and the perfect saddle (Fig. 2). These shapes are in fact non-existent in geologic data sets, as they require at least one principal curvature to precisely equal zero. Measurement error and the inherent irregularity of geologic surfaces preclude this possibility, although geologists often approximate folds as cylindrical to simplify description and analysis, knowing such perfect shapes do not exist. However, it is useful to approximate some geologic surfaces as idealized, or to quantify how far a geologic surface is from the ideal.

To allow for and quantify these approximations we utilize the curvature threshold, $k_t$, introduced by Bergbauer (2002). This threshold specifies an absolute curvature value below which calculated principal curvatures of either sign are set to zero, thereby allowing the classification of "idealized" shapes. A 2-D demonstration of this process is shown for the example of the parabola $y = x^2$ with arbitrary units of meters (Fig. 3). As $x$ goes to infinity, so do $y$ and the radius of curvature $R$, making $k = -1/R$ go to 0 (note the curvature is negative).

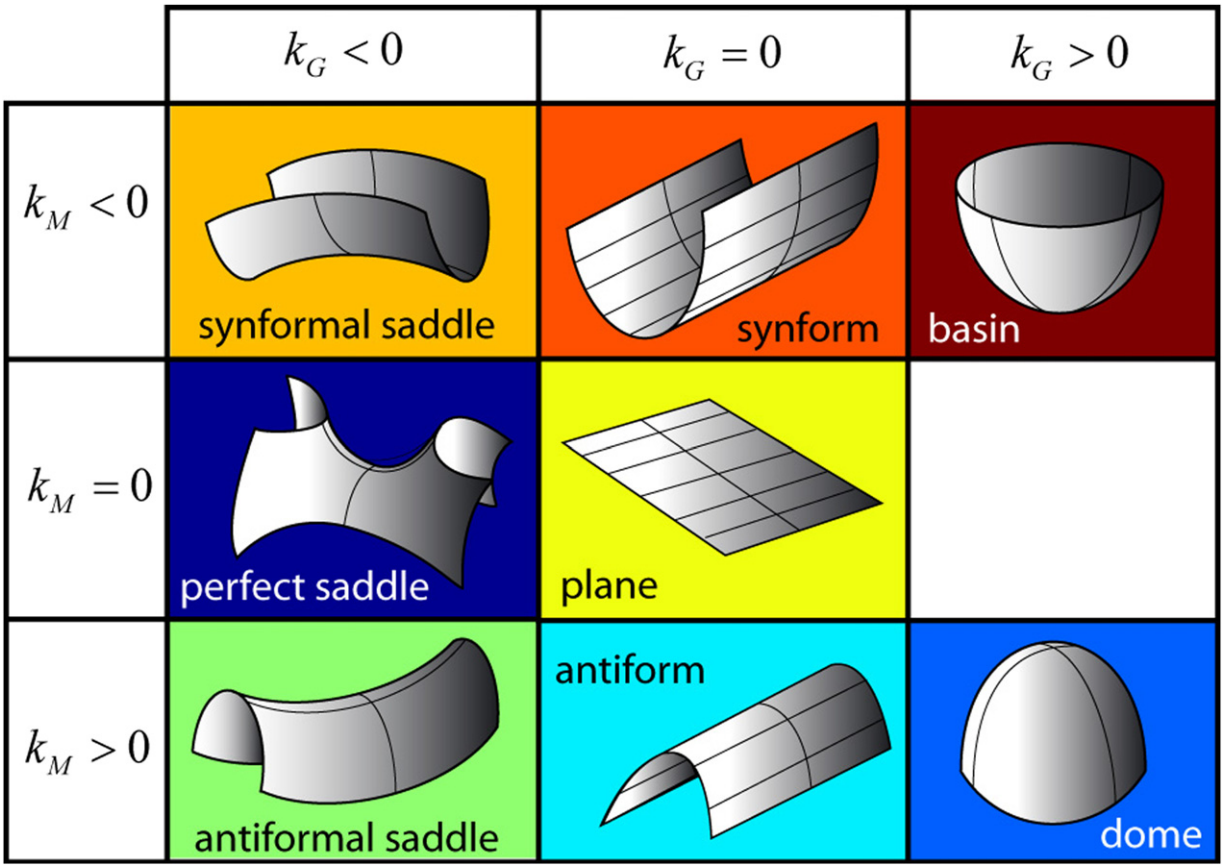


Fig. 2. Geologic curvature classification. The geologic curvature of a point on a surface can be determined from the Gaussian ($k_G$) and mean $k_M$ curvatures at the point. The color code is used throughout the paper. Modified from Roberts (2001) and Bergbauer (2002).

By specifying $k_t$, sections of the parabola can be defined as having zero curvature for subsequent analyses or calculations. For $k_t = 0.1\ m^{-1}$, all locations on the parabola with $|k| < 0.1\ m^{-1}$ ($R > 8.8$ m) are assigned a curvature of zero (light grey) and treated mathematically as linear. This isolates the sections of the parabola with greater curvature (dark grey and black) and continues to consider them parabolically curved. Making a greater approximation and setting $k_t = 0.5\ m^{-1}$ assigns sections of the parabola with $|k| < 0.5 m^{-1}$ ($R > 1.9$ m) curvature values of zero. With this approximation all light and dark grey sections are treated as linear. For a surface, this process can be used to define points as synformal, antiformal and planar.

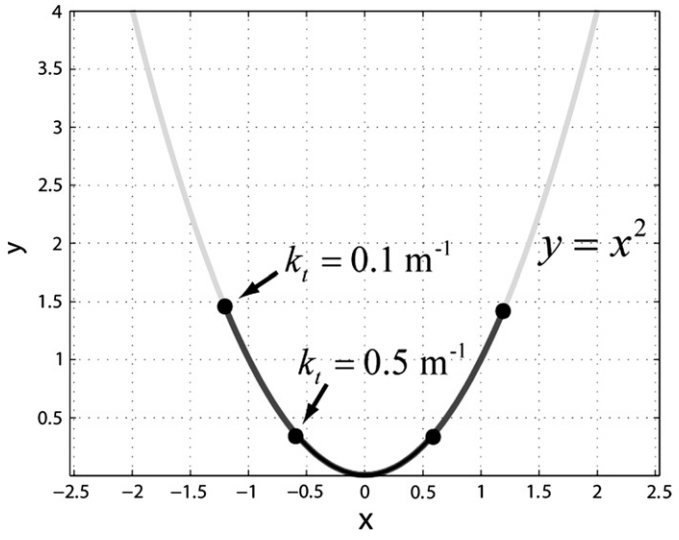


Fig. 3. Application of the curvature threshold $k_t$ to the parabola $y = x^2$. Light grey sections of the curve are treated as linear when $k_t = 0.1\ m^{-1}$ and dark grey are treated as linear when $k_t = 0.5\ m^{-1}$. In both cases the black section retains its curvature values.

In order to approximate geologic surfaces as perfect saddles (Fig. 2), a similar algorithm is applied. Recall that saddles have principal curvatures $k_{min}$ and $k_{max}$ of opposite signs, and a perfect saddle would have $k_{min} = -k_{max}$, or $k_M = 0$. The principal curvature values will never be of equal magnitude for geologic surfaces, but may be close enough to warrant this approximation. Idealized perfect saddles can therefore be specified at points where the sum $|k_{min} + k_{max}|$ falls below $k_t$.

## 3. Description of an anticlinal surface using differential geometry

### *3.1. Description of field area and creation of surface model*

Sheep Mountain anticline is a doubly plunging asymmetric fold located near Greybull, Wyoming (Forster et al., 1996;

Hennier and Spang, 1983; Savage and Cooke, 2004). The fold hinge trends NW-SE, parallel to the eastern edge of the Bighorn Basin. The NE forelimb is considerably steeper than the backlimb, and in places is vertical to slightly overturned (Bellahsen et al., 2006). A river cut perpendicular to the fold axis provides a natural cross-section and exposes sedimentary rock units aged from Mississippian to Paleocene (Thomas, 1965). The fold is interpreted to be the result of movement along an underlying thrust fault resulting from Laramide compression (Stanton and Erslev, 2004).

Forster et al. (1996) created a structure contour map of the base of the Jurassic Sundance Formation which Bellahsen et al., (2006) used to build a 3-D model of the Sheep Mountain anticline by scanning and digitizing the map using Gocad, creating ~850,000 unevenly spaced points. From these data we selected a smaller subset, limited to the NW nose of the fold, and extracted and linearly interpolated them to a 50 m grid, creating a data set of 4641 $x$, $y$ and $z$ points in a $\sim 3 \times 5$ km area. In order to examine the overall geometry of the fold and remove minor inaccuracies created by the digitizing process, a spectral filtering technique was employed to remove local surface undulations (Bergbauer et al., 2003). Using this method, all wavelengths shorter than 500 m were removed from the model surface. The final model (Fig. 4) shows the steep forelimb, tight hinge area, a shallower backlimb with several undulations parallel to the fold hinge and a tight synclinal flexure in front of the forelimb.

### 3.2. Geometric description and analysis of fold model

After creating the surface, the coefficients of the first (I) and second (II) fundamental forms were calculated at each grid point. These values quantify all geometric aspects of the fold model (Lipschultz, 1969; Pollard and Fletcher, 2005). Here we use these coefficients to calculate curvatures at each point on the model surface using Eq. (10) and examine their spatial variations.

Fig. 4a shows the distribution of maximum curvature ($k_{max}$). The anticlinal fold hinge is clearly visible as the red area of elevated $k_{max}$. Note that while the fold hinge (the line connecting points of greatest maximum curvature on serial cross sections (Marshak and Mitra, 1988) and the structural high or crest line of the fold are sub-parallel, they are not coincident. Values of $k_{max}$ vary from $9.4 \times 10^{-3}$ m$^{-1}$

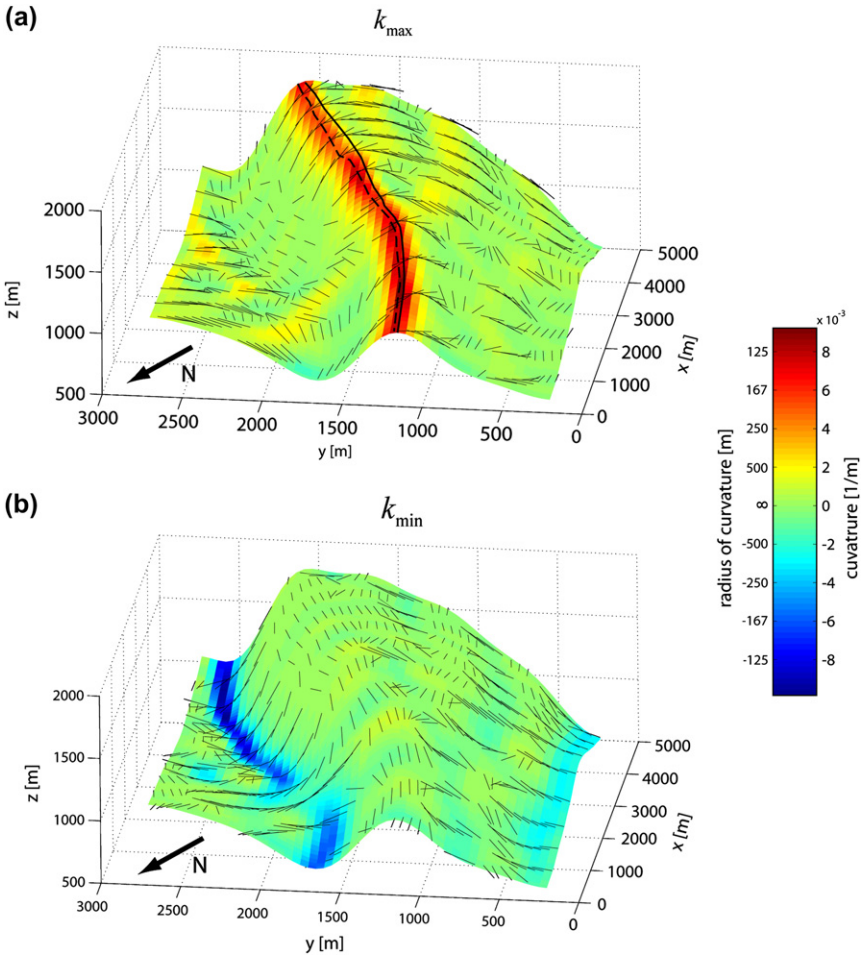


Fig. 4. Principal curvature magnitudes and directions draped on 3-D Sheep Mountain Anticline model, with magnitudes shown by colors, directions indicted by black tic marks. (a) Magnitudes and directions of $k_{max}$. Note difference between hinge line (dashed black line) determined from curvature magnitude and crest line (solid black line) determined from elevation values. (b) Magnitudes and directions of $k_{min}$.

(107 m) to $-1.0 \times 10^{-2}$ m$^{-1}$ (−100 m). These correspond to points in the anticlinal and synclinal flexures respectively. The orientations of $k_{max}$ are displayed as black tick marks across the model surface. Near the anticlinal hinge these vectors are sub-perpendicular to the hinge line, suggesting that the hinge is locally approximately cylindrical. The undulations on the backlimb sub-parallel to the hinge display similar elevated values and sub-perpendicular orientations of $k_{max}$. The orientations of $k_{max}$ in the forelimb are sub-parallel to the hinge, implying that undulations along the strike are greater than variations in curvature perpendicular to the hinge. The orientations of $k_{max}$ elsewhere on the fold reflect minor undulations superimposed upon the overall fold geometry.

Fig. 4b shows the minimum curvature ($k_{min}$), and the most obvious feature is the blue area of high magnitude negative curvature corresponding to the synclinal flexure at the base of the forelimb. Here, similar to the anticlinal hinge, the orientations of $k_{min}$ are sub-perpendicular to the synclinal hinge, again suggesting the synclinal area is locally approximately cylindrical. At the anticlinal hinge, the orientations of $k_{min}$ are parallel to the hinge line and perpendicular to the orientations of $k_{max}$. Values of $k_{min}$ range from $-1.0 \times 10^{-2}$ m$^{-1}$ (−100 m) to $1.0 \times 10^{-3}$ m$^{-1}$ (1000 m) with the most negative values corresponding to the synclinal flexure.

While it appears that the anticlinal and synclinal hinges are locally approximately cylindrical, it is evident that these portions of the fold are not cylindrical. In order for a folded surface to be ideally cylindrical, principal curvatures oriented parallel to the hinge line must be zero at each point, so a fold axis can be defined. It is evident that this requirement is not met for either hinge.

By using the concept of geologic curvature and implementing the curvature threshold ($k_t$), one can examine how far a surface departs from the cylindrical idealization. Fig. 5a shows the geologic curvature calculated across the surface with $k_t = 0$, so no principal curvatures are approximated as zero. Using the color code of Fig. 2, areas on the surface are identified as domes, basins, and antiformal and synformal saddles. As no principal curvatures are set to zero, no cylindrical or planar points appear. The anticlinal hinge of the fold and the sub-parallel undulations on the backlimb are identified as convex up domes and antiformal saddles, while the synclinal hinge is composed of basins and synformal saddles. By setting $k_t = 1 \times 10^{-4}$ m$^{-1}$ (10,000 m), small principal curvatures are approximated as 0. The result is shown in Fig. 5b, where the surface has small areas composed of cylindrical points. These are located along lines separating various non-cylindrical patches of the surface and in effect demarcate the ‘‘transition

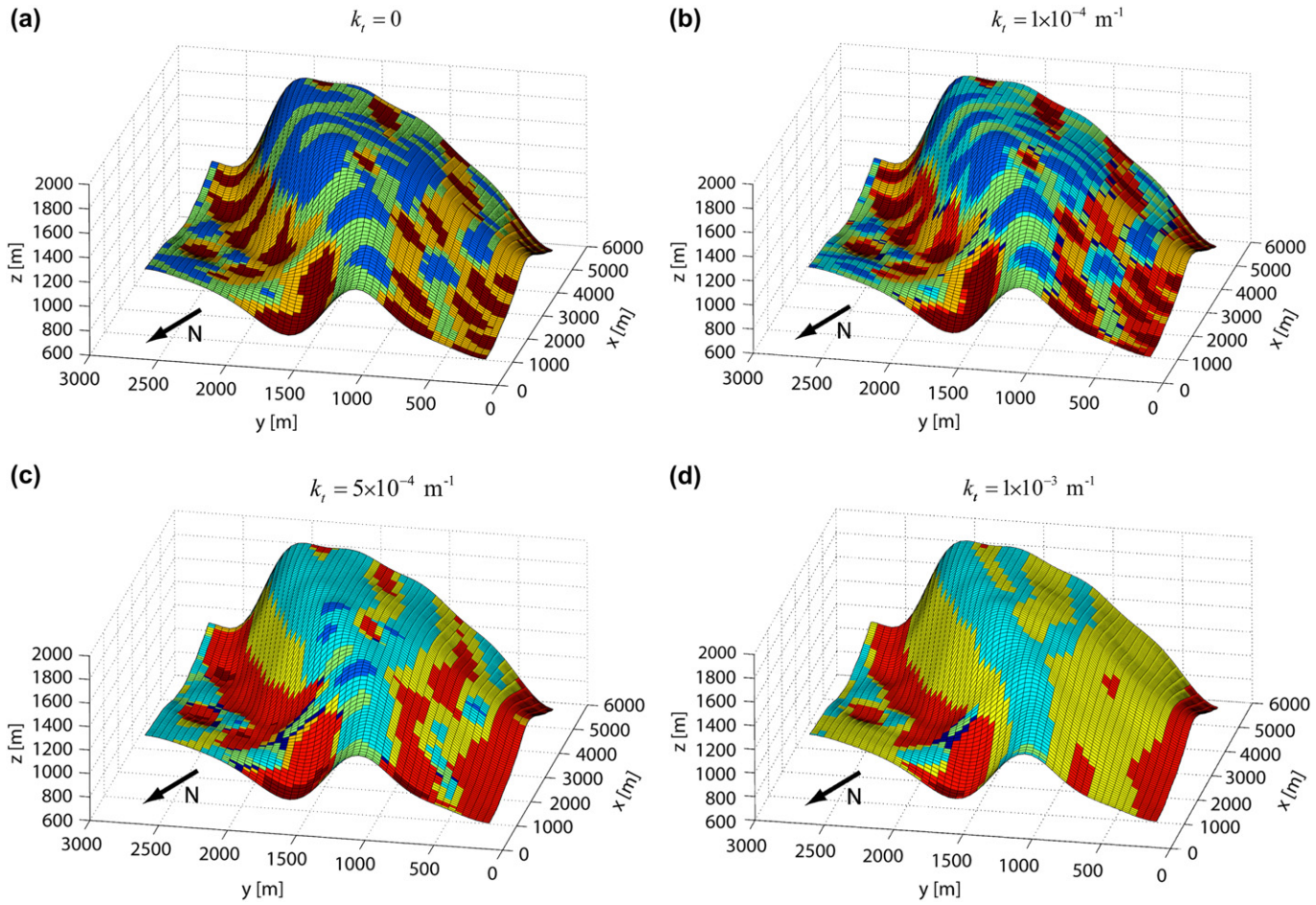


Fig. 5. Geologic curvature plotted on the Sheep Mountain Anticline model with varying values of the curvature threshold $k_t$. Colors correspond to Fig. 2.

lines'' at the intersection of these areas. For example, the points that mark the transition from dome to antiformal saddle are specified as antiformal and the points along the transition from basin to synformal saddle are synformal (see Lisle and Toimil, unpublished). Additionally, local perfect saddles are present at some points where antiformal and synformal saddles intersect.

By increasing $k_t$ to $5 \times 10^{-4}\ m^{-1}$ (2000 m) and then to $1 \times 10^{-3}\ m^{-1}$ (1000 m), increasingly larger areas of contiguous cylindrical and planar points appear (Fig. 5c,d). The smallest absolute principal curvature value on the fold model is $5.3 \times 10^{-8}\ m^{-1}$ ($1.9 \times 10^{7}$ m), so approximately five orders of magnitude of principal curvature values have been set to zero at this threshold. The anticlinal hinge and adjacent backlimb undulations are composed almost entirely of antiformal points and the synclinal hinge is composed primarily of synclinal points. Both limbs are approximated as composed predominately of planar points.

It is important to note that while individual points may be approximated as cylindrical or planar, this does not indicate that the surrounding surface is approximately cylindrical or planar in these areas. For example, while individual points classified as antiformal have one principal curvature equal to zero (Fig. 5d), the other principal curvature may not be equal to those at adjacent points parallel to the fold hinge, a requirement for cylindrical surfaces. Similarly, while individual points classified as planar have both principal curvatures equal to zero (Fig. 5d), adjacent planar points may not lie in the same plane.

Bellahsen et al. (2006) compared fracture characteristics at Sheep Mountain Anticline to the distribution of curvature across the fold. They found a fold hinge parallel, bed perpendicular fracture set generally confined to the high curvature hinge area and used this correlation to infer that the fold evolved with a fixed hinge, and that the fractures were induced by the high degree of folding related deformation in the hinge. Additionally, by examining the distribution of curvature, they found that where the set existed slightly outside the hinge area in the backlimb, curvature values were still relatively high and supported their hypothesis of bending induced fracturing.

## 4. Description of a dome-and-basin surface using differential geometry

### 4.1. Surface processing

A 3-D depth migrated seismic reflector from the North Sea (Bergbauer et al., 2003) is used to test the applicability of the tools of differential geometry for the quantitative description of non-cylindrical geological surfaces (Fig. 6). The horizon was exported from seismic interpretation software using a 25 m grid spacing, which amounts to ~129,520 grid points. Again, the surface was smoothed to eliminate undesired fault traces and data acquisition noise by removing spatial wavelengths of <2000 m (Bergbauer et al., 2003). This process left the large scale structure of the horizon which consists of a central dome surrounded by smaller basins and domes separated by saddles. The central dome is about 6 km in diameter, and rises ~150–230 m above the surrounding level of the horizon.

### 4.2. Geometric description using differential geometry

The maximum principal curvature ($k_{max}$) is positive on the crest and flanks of the domal structure while around the base of the dome the minimum principal curvature ($k_{min}$) is consistently negative (Fig. 6). At most locations on the dome crest, the signs of the two principal curvatures are positive, which is the expected signature for domal structures. Differences between the two principal curvature magnitudes at some locations on the dome are small compared to the differences observed on the anticlinal and synclinal hinges of the Sheep Mountain anticline (Fig. 4), suggesting that parts of the dome are nearly spherically shaped. Where the dome turns laterally into saddle shaped areas, the differences between the two principal curvatures increases. Similar patterns are found between smaller dome-and-basin structures to the north and south of the central dome. Two individual crestal areas showing elevated $k_{max}$ separate a smaller basinal structure located to the west of the central dome.

Calculated geologic curvature (Fig. 7a) identifies the locations of the domes and basins on the horizon which are connected by saddles. In this figure the curvature threshold ($k_t$) is set to $1.5 \times 10^{-6}\ m^{-1}$ (666,667 m), and therefore small areas of contiguous cylindrical points emerge along the transition lines between areas of non-cylindrical points. However, the surface generally contains no large areas containing cylindrical points, because neither principal curvature is close to zero over most of the horizon.

In contrast to the modeled surface of Sheep Mountain anticline (Fig. 5), the horizon from the North Sea does not decompose into extensive areas of cylindrical points when the threshold curvature is increased to $k_t = 7 \times 10^{-5}\ m^{-1}$ (14,285 m), representing approximately five orders of magnitude above the smallest absolute principal curvature value of $1.0 \times 10^{-10}\ m^{-1}$ ($1.0 \times 10^{9}$ m). Rather the pattern remains a patchwork of various antiformal, synformal and planar points (Fig. 7b). The crest of the dome is primarily composed of antiformal points; points to the north and the west are primarily planar; and points to the east and the south are primarily antiformal and synformal. Several areas of contiguous saddle points remain where the areas composed of cylindrical points intersect. Although not shown here, upon setting $k_t = 1.5 \times 10^{-4}\ m^{-1}$ (6667 m), most of the horizon is approximated by a plane. As anticipated the geometry of this dome and basin horizon from the North Sea does not reduce to a cylindrical shape, and it is evident that meaningful interpretations of geologic surfaces requires appropriate values of $k_t$.

Only those areas where both principal curvatures are positive can form a four-way closure and accumulate fluids; these areas have positive Gaussian and mean curvatures, and are therefore shaped like domes (Fig. 7). Additionally, a dome can only act as a trap if it contains a horizontal point, i.e.

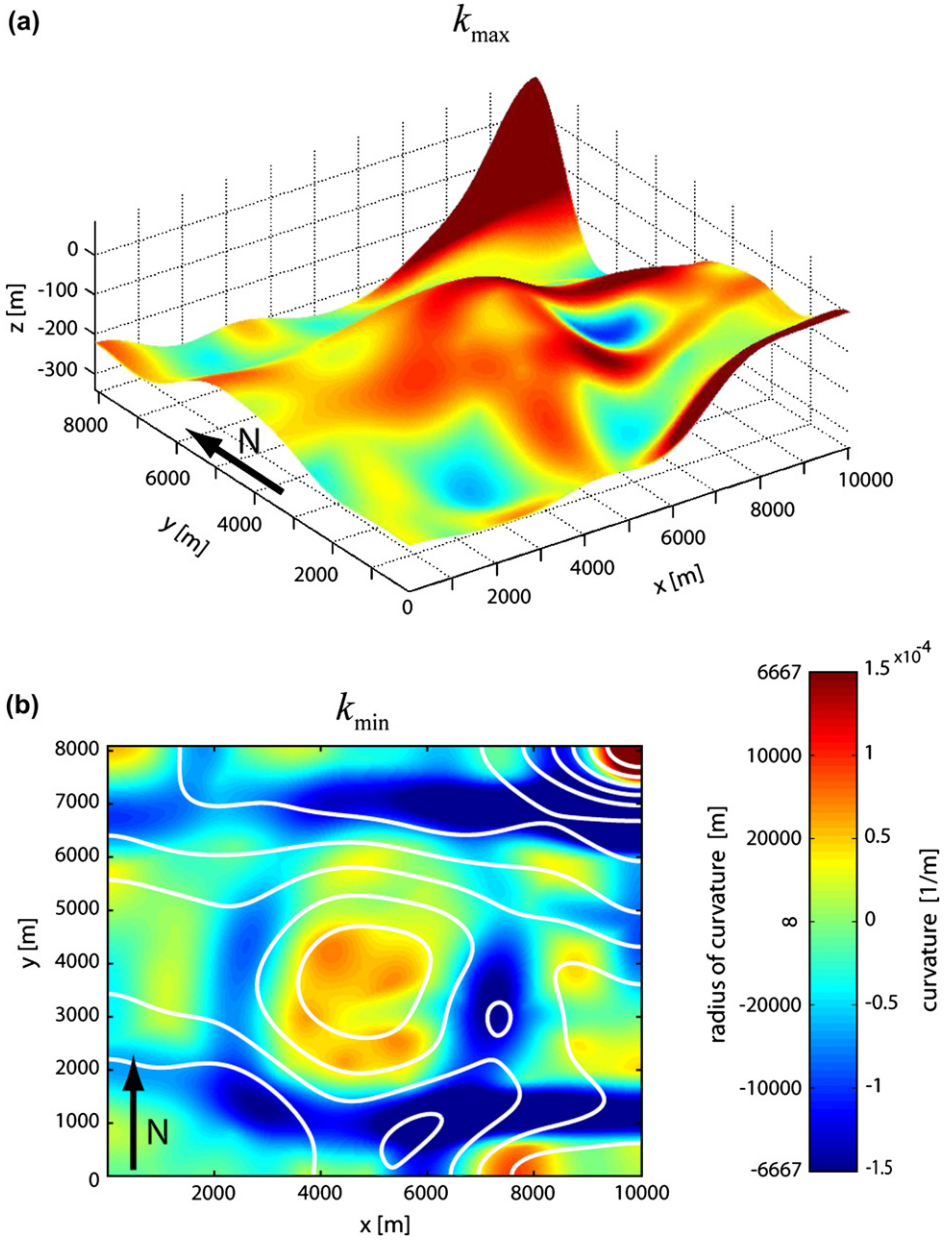


Fig. 6. Principal curvature magnitudes for 3-D depth migrated, seismically mapped horizon from the North Sea. (a) Maximum principal curvature, $k_{max}$ mapped onto oblique 3-D view of the horizon. (b) Minimum principal curvature, $k_{min}$. White lines are elevation contours.

a location where the plane tangent to the surface at the point is horizontal. The relative position of the horizontal point within the domal area provides a rough estimate of its trapping capacity: if the horizontal point is located near the edge of the domal area (e.g. the left or right half of a sphere), only small amounts of fluids can be trapped compared to a horizontal point located in the center of the domal area (e.g. the top half of a sphere). After calculating shape-curvature, domal areas containing horizontal points can be located and indicate areas of four-way closure that can trap fluids. The large dome in the North Sea structure is such an area and the horizontal point in it is centrally located and shown by black X's (Fig. 7).

The next step is to find the locations of spillpoints where fluids can escape from the area of four-way closure. These locations have negative Gaussian curvature and are defined as saddles. Within a particular saddle, the point at which leakage from the adjacent dome can occur is a horizontal point. Using this criterion, three possible spillpoints for the central dome exist. The correct spillpoint is the one of highest elevation as fluids will leak from it before they reach the lower ones. For the central dome this spillpoint is marked by red X's in Fig. 7. The volume of the dome above the elevation of the spillpoint determines the total possible volume of the reservoir. The trapped volume (including both rock and pores) under the dome is 8.44e$^8$ m$^3$ (134.2 million barrels). An upper limit of trapped fluids can be calculated from this volume given the average porosity.

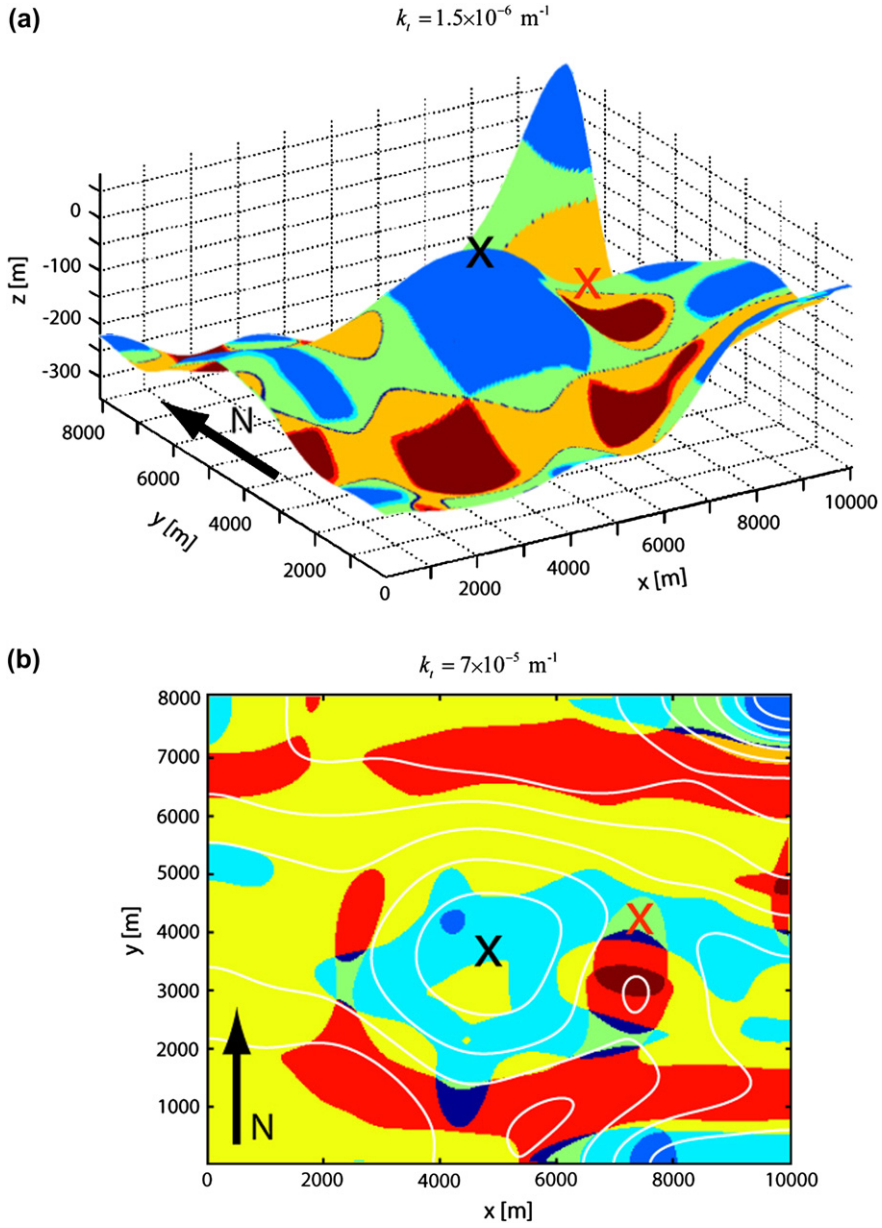


Fig. 7. Geologic curvature calculations for the North Sea horizon with varying values of the curvature threshold $k_t$. Colors indicate the local shape of the surface as in Fig. 2. Black X's denote location of horizontal point in a domal area of four-way closure. Red X's in saddles denote location of uppermost spillpoint for the large dome. White lines are elevation contours.

## 5. Discussion

While many existing methods to describe folded surfaces assume cylindricity and/or symmetry of the structure, differential geometry admits the quantitative description of any fold shape, regardless of its symmetry and spatial variations. A folded surface is completely described by the two fundamental forms of differential geometry, and various useful quantities, including arc lengths and normal curvatures, can be calculated from these. Additionally, the geologic curvature classification allows the identification and visualization of the shape and orientation of points and areas on geologic surfaces. This method segregates surfaces into areas of structural similarity and facilitates the multi-scale comparison of structural shape (e.g. antiformal saddle) to structural characteristics (e.g. fracture density). Finally, application of the curvature threshold quantifies the degree to which a point on a surface departs from an "idealized" planar, cylindrical or saddle form.

Further applications of differential geometry to structural geology are limited only by the imagination of the user. For example, these tools are ideal for the comparison of laboratory scaled models to natural folds and for testing theoretical models of folding. We demonstrate this by analyses of analogue wax models developed by Grujic et al. (2002) and viscous fold models developed in conjunction with Fletcher (1977, 1991). We point out that descriptions of analogue folds based on stereographic projections of poles to layers cannot be used to reconstruct the surface because spatial information has

been lost. Descriptions based on differential geometry are inherently tied to spatial variations. For the viscous fold models we show that the ratio of cylindrical to non-cylindrical points may be used to distinguish pure from simple shear loading conditions. These demonstrations may be downloaded at: http://pangea.stanford.edu/projects/structural_geology/chapters/chapter03/index.html.

## Acknowledgements

Thanks to Tricia Fiore and Nicolas Bellahsen for data and assistance on Sheep Mountain Anticline and to Tapan Mukerji for general technical assistance. This paper benefited greatly from detailed and thoughtful reviews by Scott Wilkerson, Richard Lisle and Bill Dunne, and from correspondence on technical issues with Richard Lisle and Mark Pearce. We thank Djordje Grujic for sharing the analogue model data and Raymond C. Fletcher for help developing the viscous fold models. This research was supported by the National Science Foundation's Tectonics Program, grant number EAR 0125935 and the Collaborations in Mathematical Geosciences program, grant number EAR 0417521, and by the Stanford Rock Fracture Project.

## References

Bellahsen, N., Fiore, P., Pollard, D.D., 2006. The role of fractures in the structural interpretation of Sheep Mountain Anticline, Wyoming. Journal of Structural Geology 28, 850–867.

Bengtson, C.A., 1981. Statistical curvature analysis techniques for structural interpretation of dipmeter data. American Association of Petroleum Geologists Bulletin 65, 312–332.

Bergbauer, S., 2002. The use of curvature for the analysis of folding and fracturing with application to the Emigrant Gap Anticline, Wyoming. PhD thesis, Stanford University.

Bergbauer, S., Mukerji, T., Hennings, P.H., 2003. Improving curvature analyses of deformed horizons using scale-dependent filtering techniques. American Association of Petroleum Geologist Bulletin 87, 1255–1272.

Bergbauer, S., Pollard, D.D., 2003. How to calculate normal curvatures of sampled geological surfaces. Journal of Structural Geology 25, 277–289.

Bevis, M., 1986. The curvature of Wadati-Benioff zones and the torsional rigidity of subducting plates. Nature 323, 52–53.

Bobillo-Ares, N.C., Bastida, F., Aller, J., 2000. On tangential longitudinal strain folding: Tectonophysics 319, 53–68.

Cloos, H., 1936. Einfuehrang in die Geologie; Ein Lehrbuch der inneren Dynamik, xii. Abhandlungen der Senckenbergischen Naturforschenden Gesellschaft 66, 503.

Davis, G.H., 1979. Laramide folding and faulting in southeastern Arizona. American Journal of Science 279, 543–569.

Dunne, W.M., 1986. Mesostructural development in detached folds; an example from West Virginia. Journal of Geology 94, 473–488.

Ekman, M., 1988. Gaussian curvature of postglacial rebound and the discovery of caves created by major earthquakes in Fennoscandia. Geophysica 24, 47–56.

Fischer, M.P., Wilkerson, M.S., 2000. Predicting the orientation of joints from fold shape: results of pseudo-three dimensional modeling and curvature analysis. Geology 28, 15–18.

Fletcher, R.C., 1977. Folding of a single viscous layer: exact infinitesimal amplitude solution. Tectonophysics 39, 593–606.

Fletcher, R.C., 1991. Mechanical analysis of large-scale folds forming above a detachment. Texas A&M University Center for Tectonophysics, College Station, TX.

Forster, A., Irmen, A.P., Vondra, C., 1996. Structural interpretation of Sheep Mountain Anticline, Bighorn Basin, Wyoming. Wyoming Geological Association Guidebook 47, 239–251.

E. Gilpin, 1883, The folding of the Carboniferous strata in the maritime provinces of Canada. Proceedings and Transactions of the Royal Society of Canada, 137–142.

Grujic, D., Walter, T.R., Gaertner, H., 2002. Shape and structure of (analogue models of) refolded layers. Journal of Structural Geology 24, 1313–1326.

Henderson, D.W., 1998. Differential Geometry: A Geometric Introduction. Prentice Hall, 250 pp.

J. Hennier, J. Spang, 1983, Mechanisms for deformation of sedimentary strata at Sheep Mountain anticline, Big Horn Basin, Wyoming. Wyoming Geological Association Guidebook 34th Annual Field Conference, pp. 97–111.

Hennings, P.H., Olson, J.E., Thompson, L.B., 2000. Combining outcrop data and three dimensional structural models to characterize fractured reservoirs: an example from Wyoming. American Association of Petroleum Geologists Bulletin 84, 830–849.

Johnson, A.M., 1977. Styles of Folding. Elsevier, New York, 406 pp.

Johnson, A.M., Fletcher, R.C., 1994. Folding of Viscous Layers. Columbia University, New York, 461 pp.

Lipschultz, M.M., 1969. Theory and Problems of Differential Geometry: Schaum's Outline. McGraw-Hill, New York, 269 pp.

Lisle, R.J., 1992. Constant bed-length folding: three-dimensional geometrical implications. Journal of Structural Geology 14, 245–252.

Lisle, R.J., 1994. Detection of zones of abnormal strains in structures using Gaussian curvature analysis. American Association of Petroleum Geologist Bulletin 78, 1811–1819.

Lisle, R.J., 2004. Geological Structures and Maps. Elsevier Butterworth-Heinmann, Burlington, MA, 106 pp.

Lisle, R.J., Fernández Martínez, J.L., 2005. Structural analysis of seismically mapped horizons using the developable surface model. AAPG Bulletin 89, 839–848.

Lisle, R.J., Robinson, J.M., 1995. The Mohr circle for curvature and its application to fold description. Journal of Structural Geology 17, 739–750.

Mallet, J.L., 2002. Geomodeling. Oxford University Press, 599 pp.

Marshak, S., Mitra, G., 1988. Basic Methods of Structural Geology. Prentice Hall, Englewood Cliffs, NJ.

Maxelon, M., Mancktelow, N.S., 2005. Three-dimensional geometry and tectonostratigraphy of the Pennine zone, Central Alps, Switzerland and Northern Italy. Earth-Science Reviews 71, 171–227.

Murray, G.H.J., 1968. Quantitative fracture study-Sanish pool, McKenzie County, North Dakota. American Association of Petroleum Geologist Bulletin 52, 57–65.

Nothard, S.D., McKenzie, D., Hains, J., Jackson, J., 1996. Gaussian curvature and the relationship between the shape and the deformation of the Tonga slab. Geophysical Journal International 127, 311–327.

Pearce, M.A., Jones, R.R., Smith, S.A.F., McCaffrey, K.J.W., Clegg, P., 2006. Numerical analysis of fold curvature using data acquired by high-precision GPS. Journal of Structural Geology 28, 1640–1646.

Pollard, D.D., Fletcher, R.C., 2005. Fundamentals of Structural Geology. Cambridge University Press, New York, 512 pp.

Ramberg, H., 1961. Relationship between concentric longitudinal strain and concentric shearing strain during folding of homogeneous sheets of rocks. American Journal of Science 259, 382–390.

Ramsay, J.G., 1967. Folding and fracturing of rocks. McGraw-Hill, New York, 568 pp.

Ramsay, J.G., Huber, M.I., 1987. The Techniques of Modern Structural Geology, Volume 2: Folds and Fractures. Academic Press, London, 391 pp.

Roberts, A., 2001. Curvature attributes and their application to 3D interpreted horizons. First Break 19, 85–100.

Samson, P., Mallet, J.L., 1997. Curvature analysis of triangulated surfaces in structural geology. Mathematical Geology 29, 391–412.

Savage, H.M., Cooke, M., 2004. The effect of non-parallel thrust fault interaction on fold pattern. Journal of Structural Geology 24, 155–172.

Stanton, H.I., Erslev, E.A., 2004. Sheep Mountain Anticline: backlimb tightening and sequential deformation in the Bighorn Basin, Wyoming. Wyoming Geological Association Guidebook 53, 75–87.

Stearns, D.W., 1969. Certain aspects of fracture in naturally deformed rocks. In: Riecker, R.E. (Ed.), Rock Mechanics Seminar. Air Force Cambridge Research Laboratory, Bedford, MA, pp. 97–118.

Stoker, J.J., 1969. Differential Geometry. Wiley-Interscience, New York, 404 pp.

Struik, D.J., 1961. Lectures on Classical Differential Geometry. Addison-Wesley, Reading, MA, 232 pp.

Suppe, J., 1983. Geometry and kinematics of fault-bend folding. American Journal of Science 283, 684–721.

Suppe, J., Medwedeff, D.A., 1990. Geometry and kinematics of fault-propagation folding. Ecologae Geologica Helvetica 83, 409–454.

A. Thomas, J.-L. Mallet, F. De Beaucourt, 1974, Une method analytique de localisation des accidents structuraux dans un massif rocheux. Proceedings of the Congress of the International Society for Rock Mechanics, pp. 625–630.

Thomas, L.E., 1965. Sedimentation and structural development of the Bighorn Basin. American Association of Petroleum Geologists Bulletin 49, 1867–1877.

Treagus, J.E., Treagus, S.H., 1981. Folds and the strain ellipsoid; a general model. Journal of Structural Geology 3, 1–17.

Wynn, T.J., Stewart, S.A., 2005. Comparative testing of ellipse-fitting algorithms: implications for analysis of strain and curvature. Journal of Structural Geology 27, 1973–1985.